Highlights of Spanish Astrophysics XI, Proceedings of the XV Scientific Meeting of the Spanish Astronomical Society held on September 4–9, 2022, in La Laguna, Spain. M. Manteiga, L. Bellot, P. Benavidez, A. de Lorenzo-Cáceres, M. A. Fuente, M. J. Martínez, M. Vázquez- Acosta, C. Dafonte (eds.), 2023

Water vapor vertical distribution in the Martian atmosphere from TGO/NOMAD observations.

Brines, A.[1], Lopez-Valverde, M.A.[1], and Sotlzenbach, A.[1] Modak, A.[1] Funke, B.[1] Galindo, F.G.[1] Aoki, S.[2,3] Villanueva, G.L.[4] Luizzi, G.[4,5] Thomas, I.[2] Erwin, J.T.[6] Grabowski, U.[6] Forget, F.[7] Lopez Moreno, J.J.[1] Rodriguez-Gomez, J.[1] Daerden, F.[2] Trompet, L.[2] Ristic, B.[2] Patel, M.R.[8] Bellucci, G.[9] and Vandaele, A.C.[2]

[1] Instituto de Astrofísica de Andalucía (IAA/CSIC), Spain
[2] Royal Belgian Institute for Space Aeronomy, Belgium
[3] Department of Complexity Science and Engineering, University of Tokyo, Japan
[4] NASA Goddard Space Flight Center, USA
[5] American University, Washington DC, USA
[6] Karlsruhe Institute of Technology, Karlsruhe, Germany
[7] Laboratoire de Météorologie Dynamique, IPSL, Paris, France
[8] Open University, UK
[9] Istituto di Astrofisica e Planetologia, Italy

Abstract

The water vapor in the Martian atmosphere plays a significant role in the planet's current and past climate, being crucial in important chemical processes like those involved in the stability of the CO_2. The recent ExoMars 2016 mission, with its NOMAD Solar Occultation channel spectrometer onboard the Trace Gas Orbiter, allowed us to measure the H_2O vertical distribution with unprecedented resolution. Recent studies of vertical profiles have shown that high dust concentration in the atmosphere, in particular during dust storms, induces an efficient transport of the H_2O to higher altitudes, from 40 km up to 80 km. Here we present the water vapor vertical distributions obtained for the Martian Years 34 and 35, covering the Global Dust Strom (GDS) event of 2018 (during MY 34) and hence, characterizing how it varies under very different dusty conditions. The direct comparison of the same season in these two consecutive Martian Years allowed us to confirm the strong impact of the GDS in the water distribution.

1 Introduction

Water vapor is present in the Martian atmosphere in relatively low abundances. Being a trace gas, its vertical distribution is affected by numerous processes, from the surface interactions to atmospheric chemistry and transport to escape to space at high altitudes.

[12]. Recent observations have proven that the ancient Mars was wetter than today, meaning that processes like the escape of water to the space have driven the planet to its current state. Also, previous works have pointed out how important is the vertical distribution of the water in the atmosphere for the evolution of the planet and for the understanding of the physical and chemical processes driving the water cycle [9]. Recent studies with the Atmospheric Chemistry Suite (ACS) and NOMAD revealed an enhancement of water vapor at high altitudes during dust events such as the Global Dust Storm during MY 34 [4, 5, 1, 2]. Other works focused on the hydrogen escape [20, 21] have suggested that the dust enhancement has a strong effect on the escape processes. Here we apply an state-of-the-art retrieval scheme to derive precise vertical profiles from NOMAD observations. Then we analyze the seasonal and latitudinal variation of the water in the atmosphere during the first half of the perihelion season of two consecutive Martian Years (MY), sampling an altitude range from the surface of the planet up to 110 km, along with an estimation of the water vapor saturation ratio.

2 NOMAD SO Measurements and Analysis

2.1 NOMAD Instrument and Dataset

The Nadir and Occultation for MArs Discovery (NOMAD) is an infrared spectrometer on-board the ExoMars Trace Gas Orbiter (TGO) that covers the spectral range between 0.2 and 4.3 μm [19]. The instrument consists of three independent channels, Limb Nadir and Occultation (LNO) operating between 2.3 and 3.8 μm, Ultraviolet and Visible Spectrometer (UVIS) operating at 200-600 nm, and Solar Occultation (SO) operating in the range between 2.3 and 4.3 μm and designed only for solar occultation measurments. This channel with a spectral resolution $\Delta\lambda/\lambda \simeq$2000, uses an echelle grating with a density of $\sim$ 4 lines/mm in a litrow configuration. It contains an Acousto-Optical Tunable Filter (AOTF) which permits to select different diffraction orders with a width that varies from 20 to 35 cm^{-1}. During each atmospheric scan, a solar occultation is measured every $\sim$1 s, allowing a vertical sampling of $\sim$1 km. In addition, the AOTF is able to change the observed diffraction order quasi-instantaneously so the SO channel can measure up to 6 diffraction orders every observation. For this study we selected a subset of measurements taken during 180° - 270° of solar longitude (L_s) during MY 34 and 35, corresponding to the first half of the Martian perihelion season. For the retrievals of water vapor we used diffraction order 134 (3011-3035 cm^{-1}) to study the the lower atmosphere (below 60 km) and order 168 (3775-3805 cm^{-1}) to study higher altitudes (above 60 km), due to the difference in the strength of the water vapor absorption lines present in these two orders. The selected dataset includes simultaneous observation of both diffraction orders, allowing us to analyze the atmosphere from $\sim$10 km above the surface up to $\sim$100 km.

2.2 Data Anaylsis and Inversion of Vertical Profiles

The NOMAD SO data used in this work are Level 1a calibrated transmittances processed at the Belgian Institute of Space Aeronomy (ISAB-BIRA) [18]. These data need to be furthermore processed in order to identify and correct for residual calibration features including spectral shifts and spectral bending across each diffraction order. At IAA we have developed tools (pre-processing phase) to clean the measured transmittances (T) corrected for the spectral shift ($\Delta\lambda$) as a proportional combination of the modeled transmittance (T_0) scaled by a factor (k), the residual bending (T_b) and the aerosol extinction along the slant path (τ). This cleaning of the data can be summarized with the following expression $T(\lambda+\Delta\lambda) = T_0^k(\lambda)\cdot T_b(\lambda)\cdot e^{-\tau}$. After this pre-processing we performed the water vapor inversion using the Retrieval Control Program (RCP), which is a fully-tested multi-parameter non-linear least squares fitting of measured and modeled spectra [22], which incorporates the state-of-the-art line-by-line radiative transfer model KOPRA (Karlsruhe Optimized Radiative transfer Algorithm) [16]. The a priori atmosphere used for RCP during the retrievals was taken from specific runs of the Mars Planetary Climate Model (LMD Mars PCM)[6], using the recent implementations of the water cycles [14] and the dust scenarios appropriate for MY 34 and 35 [10, 11]. This inversion of H_2O profiles was done with two different diffraction orders, 134 and 168. When both were measured simultaneously, in this work we built a full water vapor vertical profile merging information from order 134 below 60 km and from order 168 above.

3 Results and Discussion

3.1 Water Vapor Seasonal Variation

The maturation phase of the 2018 Global Dust Storm (GDS) occurred during L_s ~190° - 210° with a long decay phase until L_s ~270° of MY 34. In Figure 1 we show the seasonal variation of the water vapor at 50 km and 90 km for MYs 34 and 35. During the GDS maturation phase, we observe an intense peak in the water vapor volume mixing ratio (VMR) showing abundances <150 ppm at 50 km in both hemispeheres and ~50 ppm at 90 km in the Southern hemisphere. This enhancement of the water vapor at high altitudes is not present during the same period of MY 35, when a GDS was not present. At the end of the analyzed period at $L_s > 240°$ we observe a progressive increase of the water vapor abundances in the Southern hemisphere during both MYs due to the seasonal temperature increase and the sublimation of the southern polar cap, allowing more water to be present in the atmosphere.

3.2 Water Latitudinal Variation

The effects of the GDS during MY 34 in contrast with MY 35 can also be observed at different latitudes. This is shown in Figure 2. During the period of strong activity of the GDS we observe a clear increase of the water vapor VMR with the water confined mostly between 60°N and 75°S and reaching altitudes up to 80 km at mid latitudes with abundances about 150 ppm. Regardless of the poor coverage of the northern hemisphere, this same period

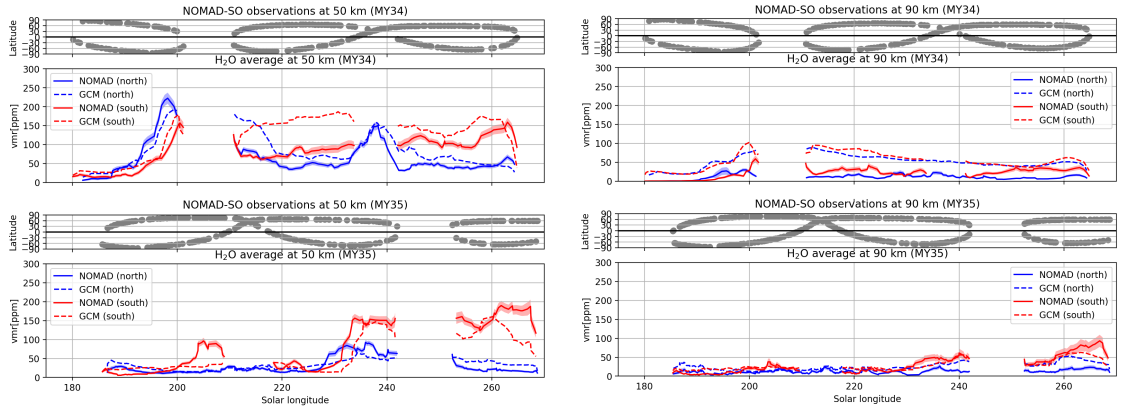

Figure 1: Seasonal variation of water vapor at 50 km (left) and 90 km (right) during L_s = 180° - 270° of MY 34 (top) and MY 35 (bottom). See text for details.

during MY 35 shows that water vapor is mostly confined below 45 km and in latitudes lower than 50°S.

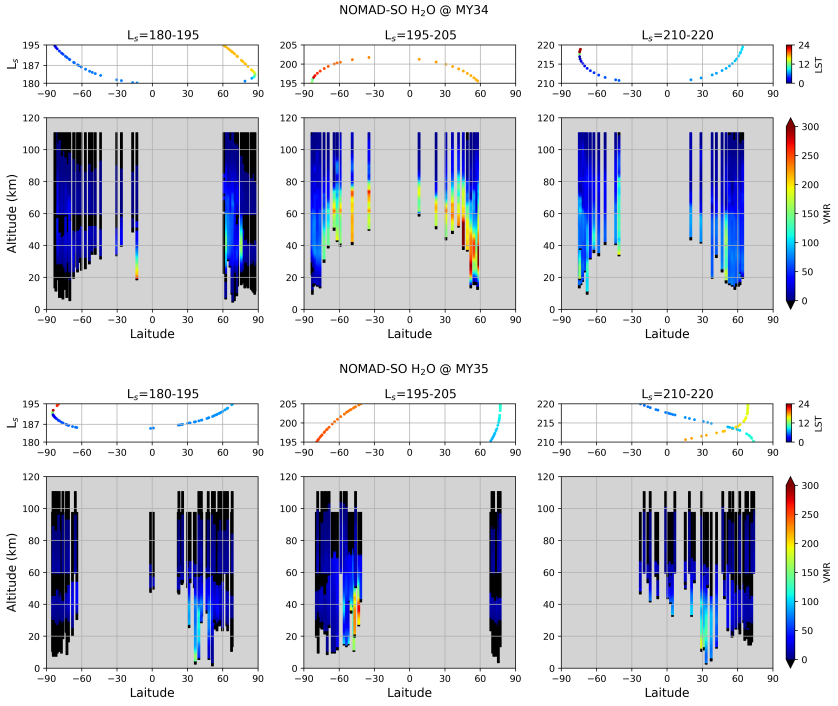

Figure 2: Latitudinal distribution of the water vapor during L_s = 180° - 220° of MY 34 (top) and MY 35 (bottom). See text for details.

3.3 Water Vapor Saturation and Water Ice

The water vapor saturation ratio (S) can be calculated as the ratio of the water vapor present in the atmosphere (retrieved water vapor μ_{H_2O}) over the expected saturated water vapor (μ_{sat}) under certain pressure and temperature conditions. In order to estimate the saturation pressure over water ice we used the well known relation of saturation vapor pressure with temperature for H_2O [13] and applied it to the NOMAD SO retrieved temperatures as obtained in our team [8], only applied when coincident retrievals of H_2O and temperature were available for MY 34. In addition, using the aerosol information obtained by [17] for the same period we identified several saturation events occurring in presence of water ice and two events of saturaiton occurring towards the top of ice clouds layers, supporting the schematic model proposed by [15]. An example of saturation in presence of water ice is shown in Figure3 (top panels) and an event of saturation observed at the top of an ice cloud is shown in Figure3 (bottom panel).

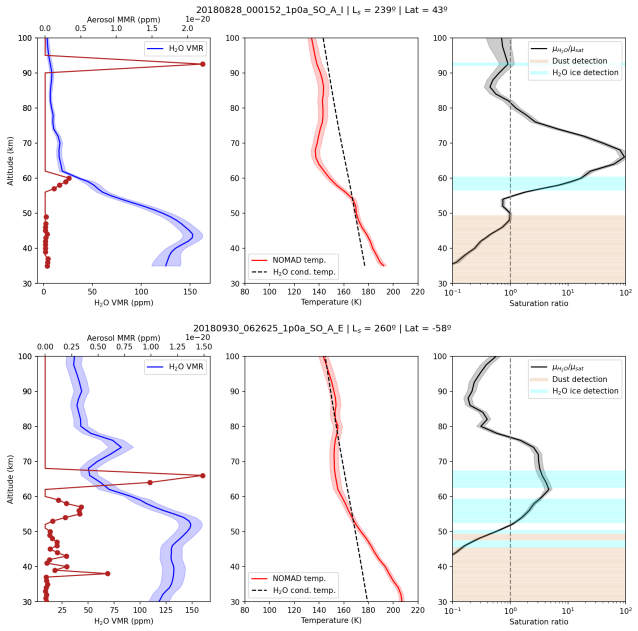

Figure 3: Profiles of water vapor, aerosols mass mixing ratio (MMR), temperature and water saturation ratio for two NOMAD SO observations. Left panels: Water vapor VMR (blue) and aerosol MMR (dark red). Center panels: NOMAD temperature (red) and water vapor condensation temperature (dashed). Right panels: Water saturation ratio (black), water ice detections (light blue) and dust detections (light brown). Vertical dashed line shows saturation ratio equal to 1. See text for details.

4 Conclusions

In this study we have presented the water vapor vertical distributions obtained for the first half of the perihelion season during Martian years 34 and 35 characterizing the water vapor under GDS and non-GDS conditions. The main results we found are:
- During the strong activity of the GDS, we observe an intense peak in the water vapor showing abundances about 150 ppm at 50 km in both hemisphere. In contrast, during MY 35, water vapor does not exceed abundances of 50 ppm above 50 km in the northern hemisphere.
- During northern winter solstice, at high southern latitudes, we observe high water vapor abundances to altitudes as high as 60 km, indicative of a progressive temperature increase. This feature is observed in both Martian Years.
- We identify saturated layers in presence of water ice, indicative of a condensation process going on at the terminator at the precise moment and local time of the NOMAD observations.
An extended version of this paper can be found in [3]. Application of these methods to an extended dataset of NOMAD solar occultations, covering the whole MY 34 and MY 35 are ongoing at our team and will be presented in future works.

Acknowledgments

The IAA/CSIC team acknowledges financial support from the State Agency for Research of the Spanish MCIU through the 'Center of Excellence Severo Ochoa' award for the Instituto de Astrofísica de Andalucía (SEV-2017-0709) and funding by grant PGC2018-101836-B-100 (MCIU/AEI/FEDER, EU) and PID2019-110689RB-I00/AEI/10.13039/501100011033 Grant PRE2019-088355 funded by MCIN/AEI/ 10.13039/501100011033 and by 'ESF Investing in your future'. F.G.G. is funded by the Spanish Ministerio de Ciencia, Innovación y Universidades, the Agencia Estatal de Investigación and EC FEDER funds under project RTI2018-100920-J-I00. ExoMars is a space mission of the European Space Agency (ESA) and Roscosmos. The NOMAD experiment is led by the Royal Belgian Institute for Space Aeronomy (IASB-BIRA), assisted by Co-PI teams from Spain (IAA-CSIC), Italy (INAF-IAPS), and the United Kingdom (Open University). This project acknowledges funding by the Belgian Science Policy Office (BELSPO), with the financial and contractual coordination by the ESA Prodex Office (PEA 4000103401, 4000121493) as well as by UK Space Agency through grants ST/V002295/1, ST/V005332/1 and ST/S00145X/1 and Italian Space Agency through grant 2018-2-HH.0. This work was supported by the Belgian Fonds de la Recherche Scientifique-FNRS under grant number 30442502 (ET-HOME). This project has received funding from the European Union's Horizon 2020 research and innovation program under grant agreement No 101004052 (RoadMap project). US investigators were supported by the National Aeronautics and Space Administration. We want to thank M. Vals, F. Momtmessin, F. Lefevre and the broad team supporting the continuous development of the LMD Mars PCM.

References

[1] Aoki, S., Vandaele, A. C., Daerden, F., Villanueva, G. L., Liuzzi, G., Thomas, I. R., ... & NOMAD team. 2019. JGR: Planets, 124(12), 3482-3497.

[2] Aoki, S., Vandaele, A. C., Daerden, F., Villanueva, G. L., Liuzzi, G., Clancy, R. T., ... & Fedorova, A. A. 2022. JGR: Planets, 127(9), e2022JE007231.

[3] Brines, A., Lopez-Valverde, M. A., Funke, B., Stolzenbach, A., Modak, A., Gonzalez-Galindo, F., et al. 2022. JGR: Planets (accepted)

[4] Fedorova, A., Bertaux, J. L., Betsis, D., Montmessin, F., Korablev, O., Maltagliati, L., & Clarke, J. 2018. Icarus, 300, 440-457.

[5] Fedorova, A. A., Montmessin, F., Korablev, O., Luginin, M., Trokhimovskiy, A., Belyaev, D. A., ... & Wilson, C. F. 2020. Science, 367(6475), 297-300.

[6] Forget, F., Hourdin, F., Fournier, R., Hourdin, C., Talagrand, O., Collins, M., ... & Huot, J. P. 1999. JGR: Planets, 104(E10), 24155-24175.

[7] Jurado Navarro, Á. A. 2016. PhD. Thesis, Univ. Granada

[8] López Valverde, M. A., Funke, B., Brines, A., Stolzenbach, A., Modak, A., Hill, B., ... & NOMAD team. 2022. JGR: Planets, e2022JE007278.

[9] Maltagliati, L., Montmessin, F., Korablev, O., Fedorova, A., Forget, F., Määttänen, A., ... & Bertaux, J. L. 2013, Icarus, 223(2), 942-962.

[10] Montabone, L., Forget, F., Millour, E., Wilson, R. J., Lewis, S. R., Cantor, B., ... & Wolff, M. J. 2015. Icarus, 251, 65-95.

[11] Montabone, L., Spiga, A., Kass, D. M., Kleinböhl, A., Forget, F., & Millour, E. 2020. JGR: Planets, 125(8), e2019JE006111.

[12] Montmessin, F., Smith, M. D., Langevin, Y., Mellon, M. T., & Fedorova, A. 2017, The atmosphere and climate of Mars, 18, 338.

[13] Murphy, D. M., & Koop, T. 2005. Quarterly Journal of the Royal Meteorological Society, 131(608), 1539-1565.

[14] Navarro, T., Madeleine, J. B., Forget, F., Spiga, A., Millour, E., Montmessin, F., & Määttänen, A. 2014. JGR: Planets, 119(7), 1479-1495.

[15] Poncin, L., Kleinböhl, A., Kass, D. M., Clancy, R. T., Aoki, S., & Vandaele, A. C. 2022. Planetary and Space Science, 212, 105390.

[16] Stiller, G. P. 2000 .Vol. FZKA 6487. Forschungszentrum Karlsruhe

[17] Stolzenbach, A., Lopez-Valverde, M. A., Funke, B., Brines, A., Modak, A., Gonzalez-Galindo, F., et al. 2022. JGR: Planets (submitted)

[18] Thomas, I. R., Aoki, S., Trompet, L., Robert, S., Depiesse, C., Willame, Y., ... & NOMAD Team. 2022. Planetary and Space Science, 218, 105411.

[19] Vandaele, A. C., Lopez-Moreno, J. J., Patel, M. R., Bellucci, G., Daerden, F., Ristic, B., ... & Wolff, M. 2018. Space Science Reviews, 214(5), 1-47.

[20] Villanueva, G. L., Liuzzi, G., Crismani, M. M., Aoki, S., Vandaele, A. C., Daerden, F., ... & NOMAD team. 2021. Science Advances, 7(7), eabc8843.

[21] Villanueva, G. L., Liuzzi, G., Aoki, S., Stone, S. W., Brines, A., Thomas, I. R., ... & Vandaele, A. C. 2022. GRL, 49(12), e2022GL098161.

[22] von Clarmann, V., Glatthor, N., Grabowski, U., Höpfner, M., Kellmann, S., Kiefer, M., ... & López-Puertas, M. 2003. JGR: Atmospheres, 108(D23).